Adaptive non-local means filtering based on local noise level for CT denoising

Zhoubo Li[1], Lifeng Yu[2], Joshua D. Trzasko[1], Joel G. Fletcher[2], Cynthia H. McCollough[2], Armando Manduca*[1]

[1]Dept. of Physiology and Biomedical Engineering

[2]Dept. of Diagnostic Radiology

Mayo Clinic, Rochester, MN 55905, USA

ABSTRACT

Radiation dose from CT scans is an increasing health concern in the practice of radiology. Higher dose scans can produce clearer images with high diagnostic quality, but may increase the potential risk of radiation-induced cancer or other side effects. Lowering radiation dose alone generally produces a noisier image and may degrade diagnostic performance. Recently, CT dose reduction based on non-local means (NLM) filtering for noise reduction has yielded promising results. However, traditional NLM denoising operates under the assumption that image noise is spatially uniform noise, while in CT images the noise level varies significantly within and across slices. Therefore, applying NLM filtering to CT data using a global filtering strength cannot achieve optimal denoising performance. In this work, we have developed a technique for efficiently estimating the local noise level for CT images, and have modified the NLM algorithm to adapt to local variations in noise level. The local noise level estimation technique matches the true noise distribution determined from multiple repetitive scans of a phantom object very well. The modified NLM algorithm provides more effective denoising of CT data throughout a volume, and may allow significant lowering of radiation dose. Both the noise map calculation and the adaptive NLM filtering can be performed in times that allow integration with the clinical workflow.

KEYWORDS

Image denoising, CT dose reduction, radiation dose reduction, non-local means filtering, spatial filtering, local noise level, noise estimation.

1. INTRODUCTION

Radiation dose from CT scanning is an increasing health concern worldwide[1]. Thus, the current guiding principle in CT clinical practice is to use radiation dose levels as low as reasonably achievable while maintaining acceptable diagnostic accuracy. However, lowering radiation dose alone generally produces a noisier image and may seriously degrade diagnostic performance. There is increasing evidence that state-of-the-art denoising algorithms may allow dose to be reduced by up to 50% in many clinical scans without compromising diagnostic performance[2-3]. Denoising algorithms can therefore play an important role in an overall strategy for reducing radiation dose.

Many denoising algorithms have been proposed for controlling noise in CT, and these can be broadly categorized into 3 major types: projection space, image space, and iterative reconstruction. Projection space techniques, which work on either the raw projection data or the log-transformed sinogram, attempt to reduce noise in the projection data domain prior to image reconstruction[4-10]. In general, these techniques have the advantage that noise properties in projection space are fairly well understood. However, they require access to the raw data and specialized knowledge, requiring either collaboration with or purchase from a manufacturer. Image-space denoising involves applying linear or non-linear filters directly to the reconstructed images. Most such techniques (e.g. bilateral filtering[11], total variation denoising[12], non-local means denoising[13], and k-SVD denoising[14] take advantage of the strong structural and statistical properties of objects in image space (e.g. sharp edges, similarities between neighboring pixels). In CT, they can be implemented directly and without access to the raw data. However, CT noise in image space is difficult to model accurately and has strong spatial variations and correlations. It can therefore be more difficult for such techniques to achieve an optimal tradeoff between

manduca@mayo.edu; phone 1 507 284-8163

Medical Imaging 2012: Physics of Medical Imaging, edited by Norbert J. Pelc, Robert M. Nishikawa, Bruce R. Whiting,
Proc. of SPIE Vol. 8313, 83131H · © 2012 SPIE · CCC code: 1605-7422/12/$18 · doi: 10.1117/12.913353

denoising and blurring or artifacts, or to get consistent performance across an entire scan volume. Iterative reconstruction (IR) techniques are more accurately considered reconstruction rather than denoising techniques, but are included here since they implicitly perform denoising. These techniques are mathematically sophisticated and take advantage of statistical assumptions about both noise properties in projection space and structure in image space[15,-17]. IR techniques require access to the raw data and accurate knowledge of the details of the scanner physics and processing, thus requiring either collaboration with or purchase from a manufacturer. True IR is very computationally intensive (e.g., several hours per data set), which has prevented clinical application to date, although software methods[18-19] and hardware methods[20-23] have been investigated to accelerate the iterative procedure. Due to the extremely high computational load of true IR, hybrid techniques have recently been developed that attempt to gain many of the benefits of true IR with much lower computational load (e.g. ASIR from GE, IRIS and SAFIRE from Siemens). Some of these are now available commercially, but integrated with the scanner.

Our interest is in a denoising strategy that can be broadly used in our own practice and across the CT community, over a heterogeneous scanner fleet that encompasses different manufacturers as well as different models of varying age and software revision. Also, most institutions do not have access to raw CT data. These requirements lead us to consider image space denoising techniques, which are relatively simple to implement, work on the image data alone, and can be applied retrospectively. As mentioned above, it is difficult for image space techniques to model CT noise or scanner details accurately, and thus they may appear to necessarily be at a disadvantage with respect to projection space or IR methods. However, the spatial structure models in some modern image denoising algorithms are significantly more advanced than the spatial regularization terms that are currently incorporated in IR. It is thus not at all clear that image space results will necessarily be inferior. Separately, we note that we also require a technique that can ultimately denoise an entire CT volume and return the results to the reader's workstation within 5 minutes, so as not to impact the clinical workflow.

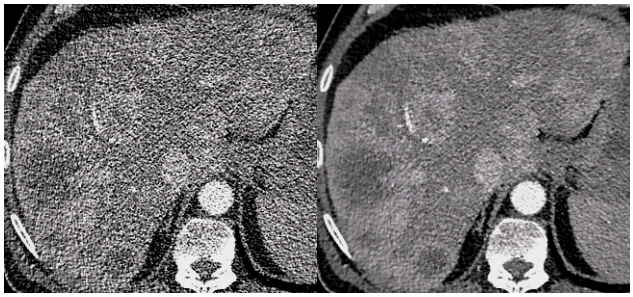

Figure 1: Closeup of an original CT slice of the abdomen and the image after NLM denoising. Note improvement in conspicuity of hepatic metastases and appearance of liver parenchyma.

Non-local means (NLM) denoising[13] is an effective image denoising strategy that exploits the inherent spatial redundancy present in most images. NLM generalizes the notion of finite spatial differences and utilizes a measure of difference between nearby image patches to estimate underlying image structure. This allows NLM to preserve a high degree of image texture and fine detail. We previously incorporated NLM denoising into the clinical CT workflow using both algorithmic and hardware speedups, such that images are returned to viewing workstations in under the 5 minute deadline[24]. However, traditional NLM uses a uniform filtering strength to denoise the image, while in CT images the noise level varies significantly within and across slices. Therefore, applying NLM filtering to CT images using a global filtering strength cannot achieve optimal denoising performance. In this work, we have developed a technique for efficiently estimating the local noise level for CT images, and have modified the NLM algorithm to adapt to local variations in noise levels.

2. METHODS

2.1 Adapting NLM to local noise level

NLM assumes that images contain a substantial amount of redundant local structure, and this property can be exploited to reduce noise by performing weighted averages of pixel intensities. The weights are based on calculations of the form

$$w(i,j) = \exp\left(-\frac{\sum_{\delta \in P} G_\sigma(\delta)[v(i+\delta) - v(j+\delta)]^2}{h^2} \right), \quad (1)$$

where G_σ is a Gaussian kernel of variance σ^2, P denotes the patch centered at positions i,j, and the weight between two pixels is calculated by computing the summed squared intensity difference of all pixels in the two patches. h is a

smoothing parameter used to control the amount of denoising and is usually taken to be proportional to the assumed or known noise level. In this work, 0.8 is used as the proportionality factor.

The original NLM, although non-iterative, usually has a high computational cost due to the computation of similarities between neighborhoods in a large search window region. In our case, we extend the NLM concept to 3D blocks in the data volume, further increasing the computational load. We have implemented and improved the pre-calculation of sum squared differences between patches using integral images[25-26], increasing the computational speed 20-fold. We have also have reduced computation time by an additional 35% by taking advantage of symmetry between weighting factors, and 30% by precalculating the exponential function in a lookup table. Finally, porting the algorithm to GPUs[24] gave an additional 35X speed gain.

In CT the noise level varies within and across slices, often by 2× within a slice and as much as 3× across slices. This implies that NLM denoising based on a single noise level may be too weak in some places (accomplishing little), too strong in others (blurring fine detail), or both. It is therefore desirable to modify the NLM algorithm to adapt to the local noise level. Adaptively denoising can overcome the problem of the non-uniform noise distribution in CT images. Here we have adjusted the strength of h locally based on an estimate of the noise level of the pixel to be denoised. This can be easily integrated with the speedup technique described above and involves little additional computational effort. However, this requires a map of the local noise level, which in turn requires developing a way to efficiently estimate such a map.

2.2 Noise map estimation

The CT image noise distribution can be estimated or calculated using many different approaches. One could repeat scans multiple times for the same object and then calculate the statistical information from reconstructed images, which is ideal but essentially impossible to implement in practice. Another approach is through Monte Carlo simulation, adding simulated noise to raw data and reconstructing multiple realizations of CT images. We have developed a highly-accurate "noise-insertion" tool, which we use with "full-dose" scans to simulate "reduced-dose" scans, based on knowledge of the physical characteristics of the scanners. The noise model used in this tool incorporates the effects of the bowtie filter, automatic exposure control, and electronic noise[10]. This tool has been validated and been used extensively in exam optimization studies[27-28], and allows us to simulate reduced-dose scans without having to re-expose patients or address interscan variations. It can also allow the calculation of accurate noise distributions in image space and yield a noise map that shows the noise level at each pixel at very high resolution. However, this method requires access to the raw data and a large number of repeated noise simulations and reconstructions, which is time consuming and makes it difficult to meet the clinical workflow requirement.

A more elegant approach is to derive the noise distribution analytically by propagating a noise model through the reconstruction equations. This has been implemented in simple fan-beam CT [29-30], where variance and covariance at each location of image space can be analytically derived, assuming a simple CT noise model. However, to analytically derive the noise formula in multi-slice helical CT, accurate knowledge of the image reconstruction process implemented in the scanner is required, which is currently not available. In addition, an accurate noise model is required for an analytical solution of the noise image. However, for the purpose of denoising using the NLM filter, an approximation of the noise map is sufficient, as noise in CT images varies smoothly in image space (Figure 2). Any noise map estimation must also be very fast (no more than a minute for an entire CT data volume) if it is to be implemented in the clinical workflow, and must be based on the CT image data alone. In this paper, we propose a simple technique, based on estimating noise in each 2D slice separately with a fan beam approximation, that does not require access to the raw data, is computationally efficient, and is easily parallelizable for speed. The basic process is described below:

i. Calculate the linear attenuation coefficient from the CT image;
ii. Generate CT sinogram data using a virtual CT geometry;
iii. Estimate the noise distribution of the sinogram data, incorporating the effect of bowtie filter and automatic tube current modulation;
iv. Apply the analytical formula to reconstruct the noise map in the final reconstructed images.

Below we explain each step in more detail.

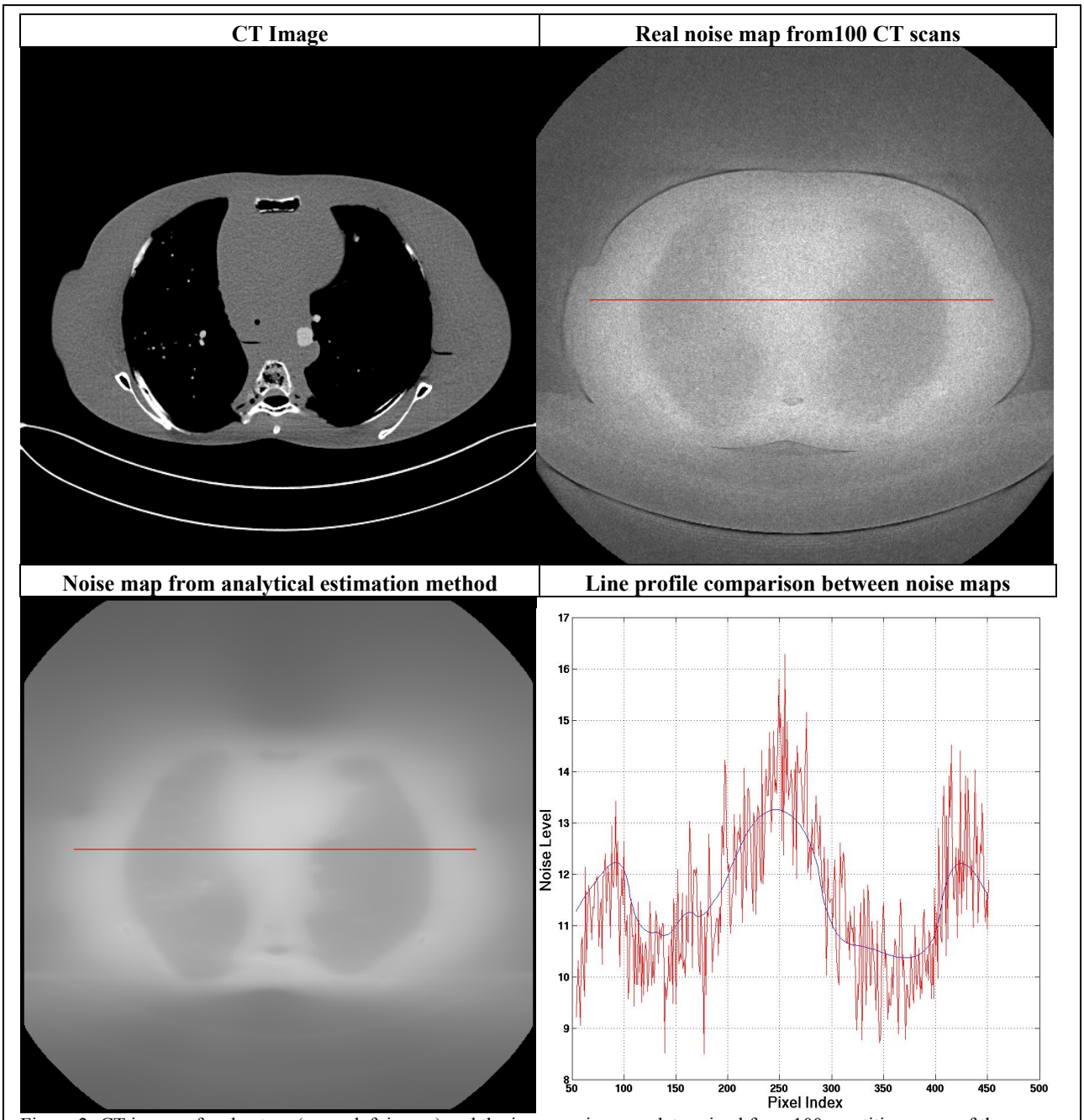

Figure 2**:** CT image of a phantom (upper left image) and the image noise map determined from 100 repetitive scans of the same phantom from a CT scanner (upper right image) and noise map estimated by analytical noise propagation through the reconstruction algorithm (lower left image). The line profiles across the two noise maps show reasonable agreement (lower right plot, jagged line: real (from 100 actual CT scans); smooth curve: simulated (image data based)).

2.3 Calculation of linear attenuation coefficient

Pixel intensities in CT images are designated in Hounsfield units (HU) which can be converted into the linear attenuation coefficient of corresponding tissues by the following equation:

$$HU = \frac{\mu - \mu(water)}{\mu(water)} \times 1000 \quad (2)$$

Here, μ refers to the linear attenuation of material with units of cm^{-1}.

2.4 Generation of CT sinogram

In principle, this requires an accurate knowledge of the CT acquisition geometry. For simplicity, in our current implementation, we used a 2D fan-beam geometry, with fan-angle and focal length consistent with the clinical scanner. A standard ray-driven or distance-driven forward projection method can be employed to generate the CT sinogram.

2.5 Noise modeling in sinogram data

Although modern CT detectors are not photon-counting elements, but rather energy integrators that generate a signal proportional to the total energy deposited in the detector, a photon-counting model is still a good approximation of quantum noise and is widely used for characterizing noise properties of CT data. As explained by[31], the bowtie filter may have a greater effect on the noise characteristics of CT data than the noise model itself. Therefore, for simplicity, we used a photon-counting model, and considered the effect of bowtie filter and tube current modulation.

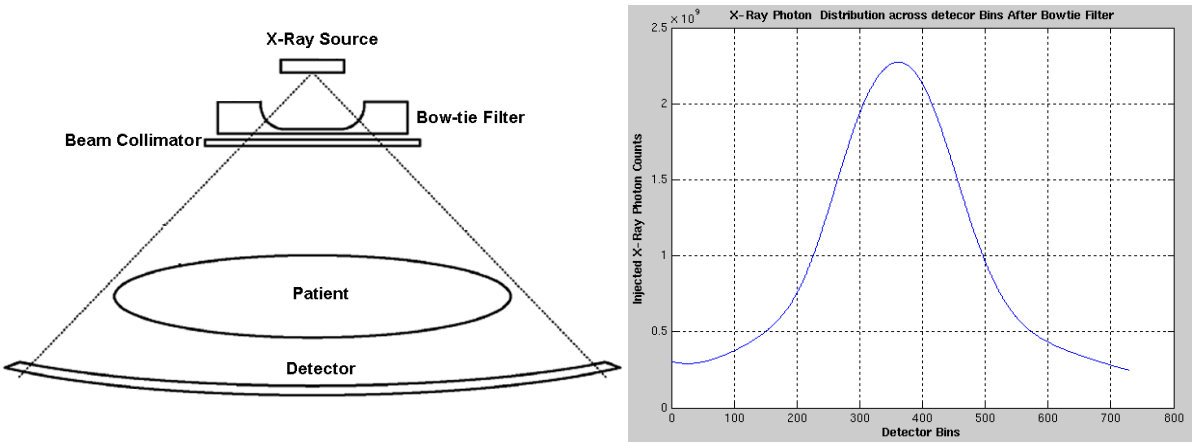

Figure 3: Illustration of a bowtie filter in a CT scanner (left) and the distribution of the incident number of photons along one detector row (right).

The effect of the bowtie filter can be characterized by measuring a map of noise-equivalent number of photons along the detector row from a set of air scans[31] (Figure 3). The tube current modulation can be estimated based on the attenuation level along each projection angle and modulation strategy described in[32]. Therefore, the incident number of photons is a function of both detector bin index and projection angle.

The incident X-ray photon number varies across the detector because of the effect of the bowtie filter. The detection of the number of transmitted X-ray photon follows a Poisson probability distribution and the variance of the detected X-ray photon is equal to its mean[33]. Therefore, once the X-ray source is determined and the incident X-ray photon number is known, a good estimation of noise variance in the projection space can be obtained by the multiplication of the incident X-ray photon number and the overall attenuation along the X-ray.

In our simulation, the input X-ray photon map can be simulated by rebinning a fan-beam X-ray photon map into the corresponding parallel projection equivalent. The attenuation map can be obtained by converting the CT image into a linear attenuation coefficient map and taking a Radon transform. Since the Radon transform is the line integration along projection lines, normally the noise in the image data does not pose a big influence on the attenuation map. The product of the incident photon map and the integral attenuation map yields the transmitted photon map. The measured integral attenuation map can be calculated by taking the natural logarithm of the ratio between the incident and the transmitted photon numbers. Assuming a Poisson distribution, the variance of the measured integral attenuation map can be calculated by[33].

$$Var(\xi,\theta) = \frac{1}{\overline{N}(\xi,\theta)} \quad (3)$$

Here, $Var(\xi,\theta)$ is the noise variance of the integral attenuation map at the ξth detector when the projection angle is θ. $\overline{N}(\xi,\theta)$ is the mean value of the detected photon numbers.

2.6 Analytical calculation of noise in reconstructed images

The derivation of an analytical formula of noise (variance and covariance) in reconstructed images requires an accurate knowledge of reconstruction algorithms, which typically involve a rebinning process to convert cone-beam data to quasi-parallel-beam data and a weighted 3D filtered backprojection (FBP) process[34]. Due to the complicated numerical operations in the reconstruction process, an accurate derivation of noise in the final image may be difficult. For the purpose of image-based NLM denoising adaptive to local noise level, it may be suffice to assume a simple CT geometry and reconstruction process. Therefore, in our current implementation, we calculated the analytical noise map based on a simple 2D fan-beam geometry and a rebinning FBP reconstruction. For further simplification and efficiency, the correlation introduced in the rebinning step was also neglected. As will be demonstrated below, these simplifications still yield a reasonably accurate noise map estimate, yet can be implemented very efficiently, which is important for this technique to be clinically viable.

Once the noise variance in the projection space is determined, the noise distribution of each pixel in the CT image can be obtained by analytically propagating the noise variance through the reconstruction algorithms. The detailed theoretical description of the parallel-beam filtered backprojection reconstruction can be found in[35] and the object function or the reconstructed image, $f(x,y)$, can be expressed as

$$f(x,y)=\int_0^{\pi} Q_\theta(x\cos\theta+y\sin\theta)d\theta \quad (4)$$

where Q_θ is called a "filtered projection" and can be written as

$$Q_\theta(\xi)=\int_{-\infty}^{+\infty} P_\theta(\xi')h(\xi-\xi')d\xi' \quad (5)$$

and $h(\xi)$ represents the spatial version of the ramp or Ram-Lak filter, $|\nu|$, and can be expressed as

$$h(\xi)=\frac{1}{2\Delta\xi^2}\frac{\sin(2\pi\xi/2\Delta\xi)}{2\pi\xi/2\Delta\xi}-\frac{1}{4\Delta\xi^2}\left(\frac{\sin(\pi\xi/2\Delta\xi)}{\pi\xi/2\Delta\xi}\right)^2 \quad (6)$$

Here, $\Delta\xi$ is the sampling interval and is equal to the interval between adjacent detectors. Practically, imaging is performed with only a finite set of view angles. Discrete analogs of (2) and (3) can be described as

$$f(x,y)=\frac{\pi}{N_p}\sum_{n=1}^{N_p}[(1-\eta(x,y,\theta_n)Q_{\theta_n}(\xi)+\eta(x,y,\theta_n)Q_{\theta_n}(\xi+\Delta\xi)] \quad (7)$$

and

$$Q_\theta(\xi)=\sum_{\xi} P_\theta(\xi')h(\xi-\xi')\Delta\xi \quad (8)$$

Here, $\eta(x,y,\theta_n)\in[0,1]$ defines the linear interpolation weight between adjacent detectors. N_p angles, $\theta_n\in[0,\pi]$, are projection angles with known projections.

The above filtered backprojection reconstruction process can be divided into three steps: filtering, interpolation and backprojection. All three processes can be treated as linear processes and the noise variance can be expressed as

$$Var(\sum_k a_k X_k)=\sum_k a_k{}^2 Var(X_k)+\sum_k\sum_{k_1\neq k} a_k a_{k1} Cov(X_k,X_{k1}) \quad (9)$$

After ramp filtering, the noise levels in the filtered projections can be written as

$$Var(Q_\theta(\xi))=\sum_{\xi}\frac{1}{\overline{N}(\xi,\theta)}h^2(\xi-\xi') \quad (10)$$

After filtering, the projection data are interpolated and backprojected into image space and the noise variance can be expressed as

$$Var(\mu(x,y))=\frac{\Delta\xi^2\pi}{N_p}\sum_{n=0}^{N_p}[(1-\eta)^2 Var(Q_{\theta_n}(\xi))+\eta^2 Var(Q_{\theta_n}(\xi+\Delta\xi)) \quad (11)$$
$$+2\eta(1-\eta)Cov(Q_{\theta_n}(\xi),Q_{\theta_n}(\xi+\Delta\xi))$$

where the covariance between the adjacent detectors can be estimated by

$$Cov(Q_{\theta_n}(\xi), Q_{\theta_n}(\xi + \Delta\xi)) = \sum_{\xi} h(\xi)h(\xi + \Delta\xi)Var^2(Q_{\theta_n}(\xi)) \quad (12)$$

Finally, the noise covariance in the CT image can be obtained after a Hounsfield-scaling by the following equation

$$Var(f(x,y)) = \frac{Var(\mu(x,y))}{\mu^2(water)} \times 1000^2(HU) \quad (13)$$

and the noise standard deviation in the CT image can be calculated by

$$\sigma(f(x,y)) = \sqrt{Var(f(x,y))} \quad (14)$$

3. RESULTS

The estimated noise map based on the 2D Radon transform of the CT image data is shown and compared with the results obtained from the real noise map from 100 repetitive scan on the same object in Fig. 2. As demonstrated, simply performing a 2D Radon transform on individual slices of the image (ignoring the true 3D cone-beam nature of the acquisition), determining the noise variance in the sinogram based on photon statistics that incorporate some of the important physical effects (in particular, the bowtie filter and automatic tube current modulation), and finally analytically propagating the noise through the reconstruction algorithm, can lead to a sufficiently close approximation to the true noise map (the black curves at the edge of the body and streaks outside the body are artifacts of the clipping of values below -1024 HU in the scanner reconstruction and are not relevant). Similar agreement is found in comparisons with obtained with the intensive noise insertion procedure described above. Currently, for a 40 cm (75 slices) CT abdomen and pelvis scan, our single threaded Matlab implementation can estimate a noise map in ~45 minutes on a dual quad-core (3.0GHz Intel® Xeon® E5472 Processors) Linux server with 32 GB shared memory. Noting the highly parallelizable

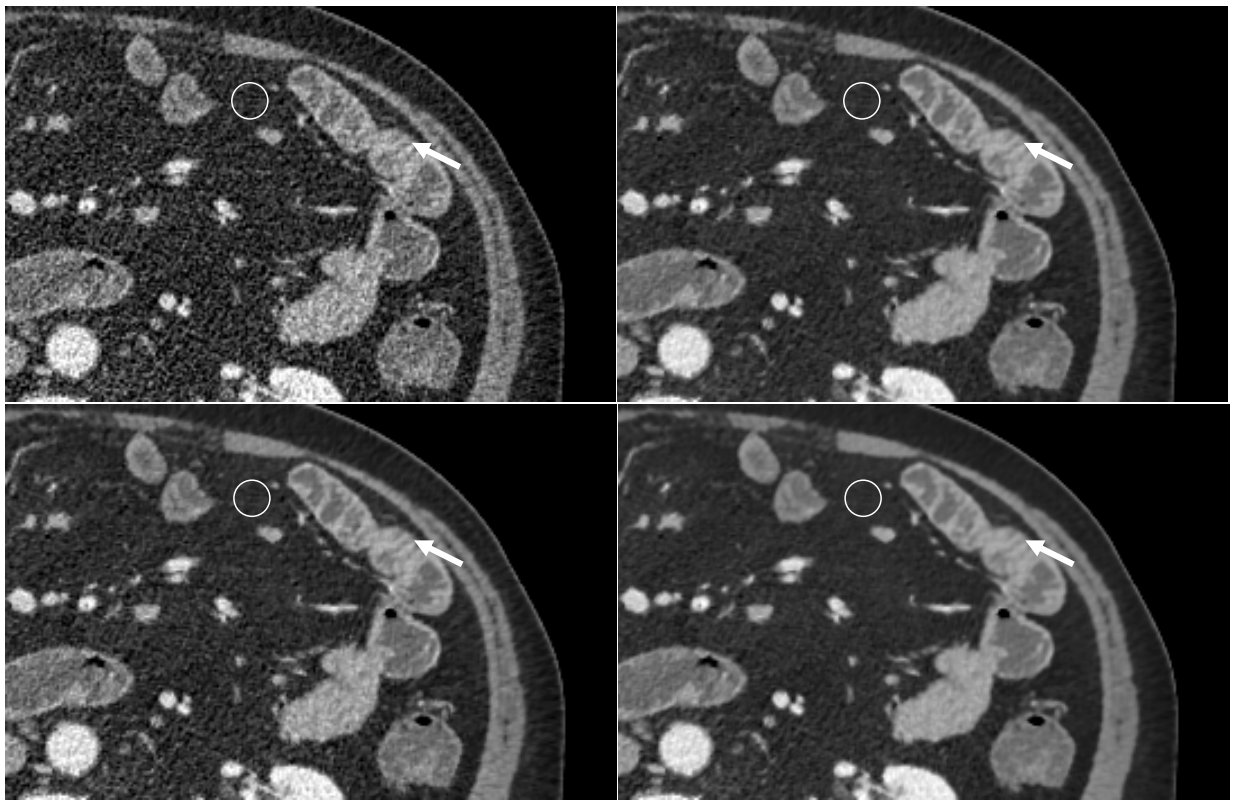

Figure 4. A section of an original half-dose abdominal CT scan (top left), denoised with the noise map technique (top right), and denoised with standard NLM with low strength (bottom left) and high strength (bottom right). The noise map and NLM at low strength give effective denoising, but NLM with high strength shows blurring of intestinal features (white arrows). The standard deviations within the ROI are 28.3, 10.6, 11.7, and 5.8 HU.

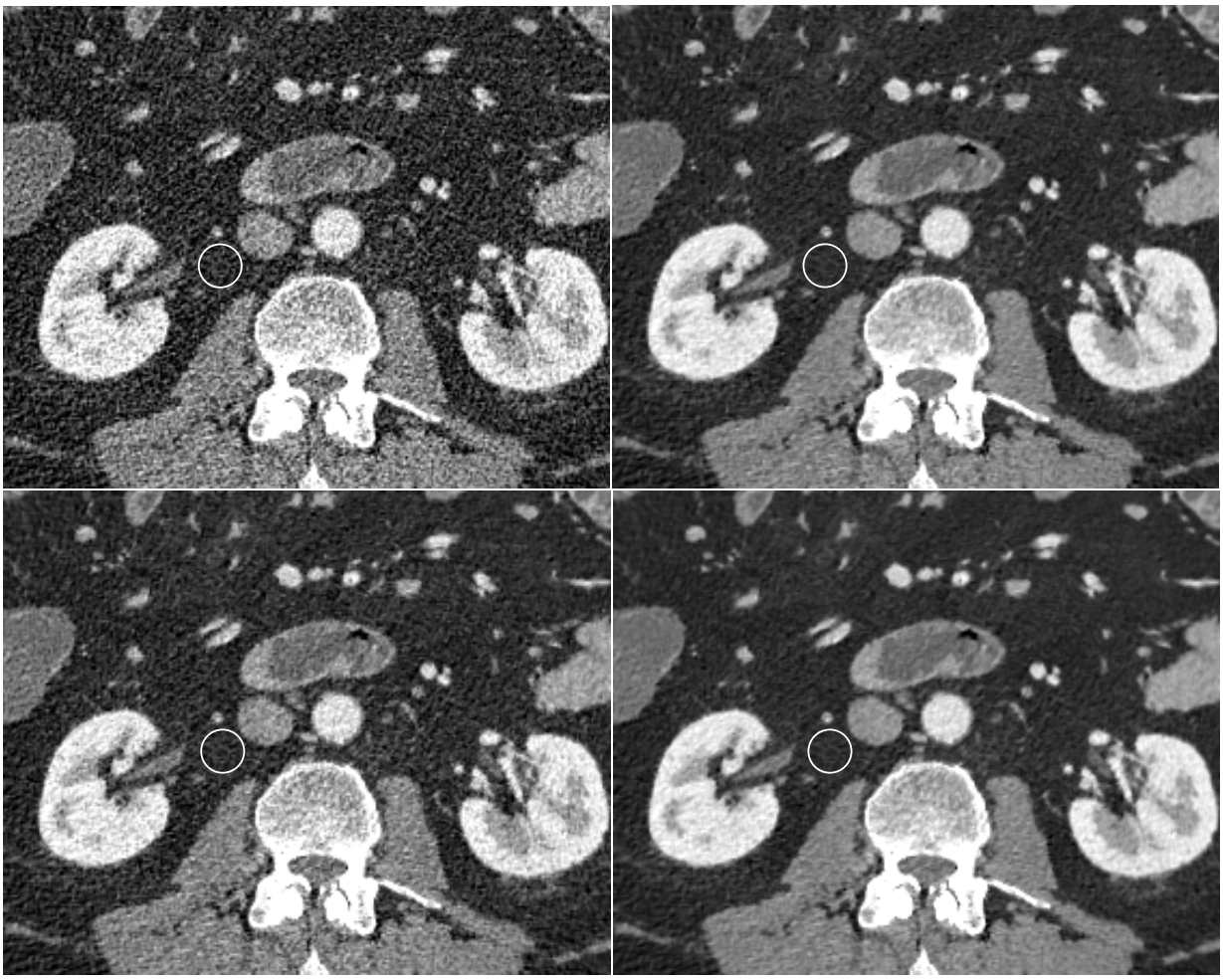

Figure 5. A different section of the same slice of the original half-dose abdominal CT scan from fig. 4 (top left), denoised with the noise map technique (top right), and denoised with standard NLM with low strength (bottom left) and high strength (bottom right). The noise map and NLM at high strength give effective denoising, but NLM with low strength gives less effective denoising. The standard deviations within the ROI are 48.3, 16.8, 29.4, and 16.2 HU.

nature of the 2D Radon transform, we anticipate that a future parallelized C implementation of this code will be substantially more efficient. Additionally, the current settings used in the simulation are 720 projections and 729 detector bins. Since the underlying noise map varies smoothly, the number of projections and detector bins can also be substantially reduced without compromising precision (data not shown here). Therefore, the ability to calculate an approximate noise map and perform noise-adaptive denoising in times that do not impact the clinical workflow appears to be feasible. Figures 4 and 5 show that the modified NLM denoising based on the local noise map is effective in two different areas of the same slice which have markedly different noise levels, whereas in fig. 4 denoising based on a fixed low strength is effective but denoising at a fixed high strength blurs intestinal features, while in fig. 5 denoising based on the fixed low strength is less effective than it could be while denoising based on the fixed high strength is effective. This continues to hold true throughout a CT volume and across patients.

4. CONCLUSIONS

We have proposed a novel approach to practically and efficiently estimate a local noise map from a CT image and shown that it agrees well with the result from multiple scans of the same object on a CT scanner. We have also modified the NLM algorithm to adaptively denoise CT images based a local noise level map with only marginal additional computational cost. The adaptive NLM filter based on the estimated noise map significantly improves both inter- and

intra-slice (and inter-patient) denoising performance. A complete evaluation of the denoising performance after incorporating the noise map is currently under way.

REFERENCES

[1] D. J. Brenner and E. J. Hall, "Computed tomography--an increasing source of radiation exposure," N Engl J Med. 357, 2277-84 (2007).

[2] M. Bai, J. Chen, R. Raupach, C. Suess, Y. Tao and M. Peng, "Effect of nonlinear three-dimensional optimized reconstruction algorithm filter on image quality and radiation dose: validation on phantoms," Med Phys. 36, 95-7 (2009).

[3] L. S. Guimaraes, J. G. Fletcher, L. Yu, J. E. Huprich, J. L. Fidler, A. Manduca, J. C. Ramirez-Giraldo, D. R. Holmes, Jr. and C. H. McCollough, "Feasibility of dose reduction using novel denoising techniques for low kV (80 kV) CT enterography: optimization and validation," Acad Radiol. 17, 1203-10 (2010).

[4] J. Hsieh, "Adaptive streak artifact reduction in computed tomography resulting from excessive x-ray photon noise," Med Phys 25, 2139–2147 (1998).

[5] M. Kachelrieß, O. Watzke, and W. A. Kalender, "Generalized multi-dimensional adaptive filtering for conventional and spiral single-slice, multi-slice, and cone-beam CT," Medical Physics 28, 475 (2001).

[6] Tianfang Li, Xiang Li, Jing Wang, Junhai Wen, Hongbing Lu, Jiang Hsieh, and Zhengrong Liang, "Nonlinear sinogram smoothing for low-dose X-ray CT," IEEE Transactions on Nuclear Science 51, 2505– 2513 (2004).

[7] Jing Wang, Tianfang Li, Hongbing Lu, and Zhengrong Liang, "Penalized weighted least-squares approach to sinogram noise reduction and image reconstruction for low-dose X-ray computed tomography," IEEE Transactions on Medical Imaging 25, 1272–1283 (2006).

[8] P. J. La Rivière, "Penalized-likelihood sinogram smoothing for low-dose CT," Medical Physics 32, 1676 (2005).

[9] P. J. La Riviere, Junguo Bian, and P. A. Vargas, "Penalized-likelihood sinogram restoration for computed tomography," IEEE Transactions on Medical Imaging 25, 1022–1036 (2006).

[10] A. Manduca, L. Yu, J. D. Trzasko, N. Khaylova, J. M. Kofler, C. M. McCollough, and J. G. Fletcher, "Projection space denoising with bilateral filtering and CT noise modeling for dose reduction in CT," Medical Physics 36, 4911 (2009).

[11] C. Tomasi and R. Manduchi, "Bilateral filtering for gray and color images," in Sixth International Conference on Computer Vision, 1998, pp. 839–846, (1998).

[12] L. I. Rudin, S. Osher, and E. Fatemi, "Nonlinear total variation based noise removal algorithms," Physica D: Nonlinear Phenomena 60, 259–268 (1992).

[13] A. Buades, B. Coll, and J. M. Morel, "A Review of Image Denoising Algorithms, with a New One," Multiscale Modeling & Simulation 4, 490 (2005).

[14] Aharon, M. Elad, and A. Bruckstein, "K-SVD: An algorithm for designing overcomplete dictionaries for sparse representation," IEEE Transactions on Signal Processing 54, 4311–4322 (2006).

[15] K. Lange and J. A. Fessler, "Globally convergent algorithms for maximum a posteriori transmission tomography," IEEE Transactions on Image Processing 4, 1430–1438 (1995).

[16] J. Nuyts, B. D. Man, P. Dupont, M. Defrise, P. Suetens, and L. Mortelmans, "Iterative reconstruction for helical CT: a simulation study," Physics in Medicine and Biology 43, 729–737 (1998).

[17] J.-B. Thibault, K. D. Sauer, C. A. Bouman, and J. Hsieh, "A three-dimensional statistical approach to improved image quality for multislice helical CT," Med Phys 34, 4526–4544 (2007).

[18] J. A. Fessler, E. P. Ficaro, N. H. Clinthorne, and K. Lange, "Grouped-coordinate ascent algorithms for penalized-likelihood transmission image reconstruction," IEEE Trans Med Imaging 16, 166–175 (1997).

[19] F. J. Beekman and C. Kamphuis, "Ordered subset reconstruction for x-ray CT," Physics in Medicine and Biology 46, 1835–1844 (2001).

[20] Fang Xu and K. Mueller, "Accelerating popular tomographic reconstruction algorithms on commodity PC graphics hardware," IEEE Transactions on Nuclear Science 52, 654– 663 (2005).

[21] J. S. Kole and F. J. Beekman, "Evaluation of accelerated iterative x-ray CT image reconstruction using floating point graphics hardware," Phys Med Biol 51, 875–889 (2006).

[22] F. Xu and K. Mueller, “Real-time 3D computed tomographic reconstruction using commodity graphics hardware,” Phys Med Biol 52, 3405–3419 (2007).

[23] M. Kachelriess, M. Knaup, and O. Bockenbach, “Hyperfast parallel-beam and cone-beam backprojection using the cell general purpose hardware,” Med Phys 34, 1474–1486 (2007).

[24] D. J. Blezek, Z. Li, B. J. Bartholmai, A. Manduca, B. J. Erickson, “Clinically Feasible CT Denoising Using a GPU-based Non-local Means Algorithm”, Society for Imaging Informatics in Medicine, 2011 annual meeting, (2011).

[25] J. Darbon, A. Cunha, T. F. Chan, S. Osher, and G. J. Jensen, “Fast nonlocal filtering applied to electron cryomicroscopy,” in 5th IEEE International Symposium on Biomedical Imaging: From Nano to Macro, 2008. ISBI 2008, pp. 1331–1334, (2008).

[26] Y.-L. Liu, J. Wang, X. Chen, Y.-W. Guo, and Q.-S. Peng, “A Robust and Fast Non-Local Means Algorithm for Image Denoising,” Journal of Computer Science and Technology 23, 270–279 (2008).

[27] L. Yu, M. R. Bruesewitz, K. B. Thomas, J. G. Fletcher, J. M. Kofler, and C. H. McCollough, “Optimal Tube Potential for Radiation Dose Reduction in Pediatric CT: Principles, Clinical Implementations, and Pitfalls,” Radiographics 31, 835–848 (2011).

[28] A. Apel, J. G. Fletcher, J. L. Fidler, D. M. Hough, L. Yu, L. S. Guimaraes, M. E. Bellemann, C. H. McCollough, D. R. Holmes, et al., “Pilot multi-reader study demonstrating potential for dose reduction in dual energy hepatic CT using non-linear blending of mixed kV image datasets,” European Radiology 21, 644–652 (2010).

[29] X. Pan and L. Yu, “Image reconstruction with shift-variant filtration and its implication for noise and resolution properties in fan-beam computed tomography,” Med Phys 30, 590–600 (2003).

[30] A. Wunderlich and F. Noo, “Image covariance and lesion detectability in direct fan-beam x-ray computed tomography,” Physics in Medicine and Biology 53, 2471–2493 (2008).

[31] B. R. Whiting, P. Massoumzadeh, O. A. Earl, J. A. O’Sullivan, D. L. Snyder, and J. F. Williamson, “Properties of preprocessed sinogram data in x-ray computed tomography,” Medical Physics 33, 3290 (2006).

[32] M. Gies, W. A. Kalender, H. Wolf, and C. Suess, “Dose reduction in CT by anatomically adapted tube current modulation. I. Simulation studies,” Med Phys 26, 2235–2247 (1999).

[33] Y. Zhang and R. Ning, “Investigation of image noise in cone-beam CT imaging due to photon counting statistics with the Feldkamp algorithm by computer simulations,” Journal of X-Ray Science and Technology 16, 143–158 (2008).

[34] K. Stierstorfer, A. Rauscher, J. Boese, H. Bruder, S. Schaller, and T. Flohr, “Weighted FBP--a simple approximate 3D FBP algorithm for multislice spiral CT with good dose usage for arbitrary pitch,” Phys Med Biol 49, 2209–2218 (2004).

[35] A. C. Kak and Malcolm Slaney, [Principles of Computerized Tomographic Imaging], Society of Industrial and Applied Mathematics, 49-75 (2001).